Restoration Method for Spatially Variant Blurred Images

Saima Ben Hadj, Laure Blanc-Féraud

INSTITUT NATIONAL DE RECHERCHE EN INFORMATIQUE ET EN AUTOMATIQUE

Restoration Method for Spatially Variant Blurred Images

Saima Ben Hadj — Laure Blanc-Féraud

N° 7654

June 2011

Vision, Perception and Multimedia Understanding

ISSN 0249-6399 ISRN INRIA/RR--7654--FR+ENG

INSTITUT NATIONAL
DE RECHERCHE
EN INFORMATIQUE
ET EN AUTOMATIQUE

INRIA

centre de recherche
SOPHIA ANTIPOLIS - MÉDITERRANÉE

Restoration Method for Spatially Variant Blurred Images

Saima Ben Hadj*, Laure Blanc-Féraud *

Theme : Vision, Perception and Multimedia Understanding
Équipes-Projets Ariana

Rapport de recherche n° 7654 — June 2011 — 32 pages

Abstract: Most of existing image restoration techniques suppose that the blur is spatially-invariant. However, various physical phenomena related to the optical instrument properties make that degradations may change in the image domain. Taking into account space-variance of optical aberrations in the restoration process is an important task that should enhance the accuracy of the estimated object. This latter issue has received little attention by researchers in these last years. In this work, we derive a restoration method for spatially-variant blurred images. In our approach, we consider a blur modeled by a space-varying linear combination of spatially invariant blurs. We develop the example of a piecewise-constant PSF model with regular transitions between areas in order to alleviate blur alteration effect. Furthermore, we develop for this model, an appropriate deconvolution method based on minimization of a criterion with total variation regularization. For this purpose, we fit a domain decomposition-based minimization approach that was recently developed by Fornassier et al., 2009 to the deconvolution problem with a spatially varying PSF model. We thus obtain a fast restoration algorithm where the true image estimation is performed in a parallel way on different sub-regions of the image. We also study the convergence of the proposed method especially for the considered spatially varying PSF model.

Key-words: Deconvolution, energy minimization, spatially-variant PSF, total variation.

* Ariana Research Group, CNRS/INRIA/UNSA, 2004, route des Lucioles, BP 93, 06902 Sophia Antipolis Cedex, France

Centre de recherche INRIA Sophia Antipolis – Méditerranée
2004, route des Lucioles, BP 93, 06902 Sophia Antipolis Cedex
Téléphone : +33 4 92 38 77 77 — Télécopie : +33 4 92 38 77 65

Méthode de restauration d'image avec un flou spatialement variant

Résumé : La plupart des techniques de restauration d'image existantes suppose que le flou est spatialement invariant. Cependant, différents phénomènes physiques liés aux propriétés des instruments optiques font que les dégradations peuvent changer dans le domaine de l'image. Prendre en compte la variation spatiale des aberrations optiques dans le processus de restauration est une tâche importante qui devrait améliorer la précision de l'objet estimé. Ce dernier problème a reçu peu d'attention par les chercheurs ces dernières années. Dans ce travail, nous développons une méthode de restauration d'image avec un flou spatialement variant. Dans notre approche, nous considérons un flou modélisé par une combinaison linéaire spatialement variante de fonctions de flou spatialement invariant. Nous développons l'exemple d'une PSF constante par morceau avec des transitions régulières entre les régions afin d'atténuer l'effet de changement de flou entre les zones. En outre, nous développons pour ce modèle, une méthode de déconvolution appropriée par minimisation d'un critère avec une régularisation par variation totale. Pour cela, nous adaptons une méthode de minimisation fondée sur une stratégie de décomposition de l'image qui a été récemment développée par Fornasier et al., 2009 au problème de déconvolution avec une PSF spatialement variante. Nous obtenons ainsi un algorithme de restauration rapide où l'estimation de l'image est effectuée d'une manière parallèle sur les différents sous-domaines de l'image. Nous étudions également la convergence de la méthode proposée notamment pour le modèle de PSF spatialement variante considéré.

Mots-clés : Déconvolution, minimisation d'énergie, PSF spatialement variante, variation totale.

Contents

1 Introduction

Since the first telescopes invented in the XVth century, optical imaging systems recognized a considerable advance providing high resolution and good contrast photography. Nevertheless, till now they suffer from some artifacts mainly due to the inherent limitations of the optical instruments as well as the imaging environment. Indeed, optical images are affected by undesired blur which is introduced by different distortion sources. For instance, the diffraction of light through a small circular aperture or imperfect optical lens produces a blur commonly represented by an Airy disc (Pawley [2006]) which limits the resolution of the acquired image. Defocus is an other example of optical aberrations. It refers to a shift of the image plane from the plane of focus and leads to the loss of small details. This kind of blur usually appears in biological images acquired by a 3D confocal laser scanning microscope, namely when the light coming from out of focus planes interferes with that coming from the target plane during the fluorescence of the excited molecules. Furthermore, camera or object motions during the exposure distort the quality of the acquired image and reduce its accuracy. In order to remove this blur and retrieve the original scene, many image restoration methods were previously developed in the literature. In most of them, the blur was supposed to be spatially-invariant, so that the image formation process can be modeled by a convolution with a function describing the imaging system blur. This function is conventionally called point spread function (PSF). It refers to the response of the imaging system to the Dirac impulse. Thus, the mathematical expression corresponding to such an observation model is given by the following equation:

$$g(x) = \sum_{t \in \mathcal{R}} \left[h(x-t) . u(t) \right] + b(x) \tag{1}$$

where $h(.)$ denotes the point spread function, assumed to be shift-invariant, $u(.)$ is the intensity of the original image to be estimated from observations $g(.)$, $b(.)$ is an additive noise (e.g. Gaussian noise) and variables x and t represent positions in the 2D or 3D discrete space $\mathcal{R}$, with $\mathcal{R}$ an open bounded set of $\mathbb{R}^2$ or $\mathbb{R}^3$.

When the point spread function is considered as spatially-invariant, the restoration of the image can be achieved using classical deconvolution methods such as Wiener filter (Pratt [1972]) and Richardson-Lucy based-algorithms (Demoment [1989], Rudin and Osher [1994]). Different regularization techniques such as total variation (Rudin et al. [1992], Rudin and Osher [1994]) or wavelet regularisation (Bect et al. [2004], Daubechies et al. [2004], Figueiredo and Nowak [2003]) were introduced in the deconvolution process according

to the considered application in order to regularize the ill-posed inverse problem. Thanks to the space invariance-assumption of the PSF, mathematical computations can be carried out in the Fourier domain so that computational cost of the convolution operation in the spatial domain is avoided.

Nevertheless, in many practical cases, the blur could not be considered as invariant in the whole image domain and it is not the same at every point of the observed scene. This issue can be encountered in several situations. For instance, imaging a scene that contains several objects placed at different focal distances w.r.t. the lens position usually leads to a varying defocus blur. Besides, a space-varying blur can also occur if we would take into account geometrical aberrations induced by the imperfect lens system or by the refractive index mismatch between the different system mediums in microscopy. For example, confocal laser scanning microscope suffers from a depth-varying blur which is mainly caused by optical aberrations of lenses. Such a phenomenon is illustrated for example in (Shaevitz and Fletcher [2007]). Astronomical and satellite images are likewise distorted with a spatially-varying blur due to atmospheric turbulence. In addition, a varying motion blur can be observed when the imaged particles move with different speeds or follow different trajectories. It is thus important to develop a restoration method for spatially-varying blurred images. Indeed, the image formation model cannot be represented anymore by a convolution between the PSF and the original image since the space-invariance blur is no longer a valid assumption. The mathematical observation model is henceforth expressed as follows:

$$g(x) = \sum_{t \in \mathcal{R}} \left[h_x(x-t) . u(t) \right] + b(x) \tag{2}$$

where $h_x(.)$ is the PSF corresponding to the location x. Because of the space-variance of the PSF, the evaluation of such operation cannot be done with a fast Fourier transform. Computations in the spatial space are very expansive in terms of CPU time and memory. In order to speed up the computational time, most of the existing methods are carried out under the assumption of local invariance of the PSF. The image space is thus sectioned into sub-regions where the blur variations are negligible so that the PSF can be considered as invariant in that sub-region. Among these methods that have dealt with the restoration problem of space-varying blurred images, we list the followings:

First, the iterative image restoration method proposed in (Nagy and O'Leary [1998]) for atmospherically blurred images is one of the earliest space-variant deconvolution techniques. It is based on the preconditioned conjugate gradient algorithm (Nagy et al. [1996]). In that method, a block-invariant blur approximation with linear interpolation of the local PSF was

considered in order to alleviate the block effect. In addition, the proposed method was extended later by Bardsley et al. (Bardsley et al. [2006]) to achieve blind restoration of spatially-varying blurred images and was particularly applied to restore astronomical images.

Besides, a non-linear restoration method based on self-organizing neural network was proposed in (Sung and Choi [1998]) to remove spatially-varying optical blur. In that method, an overlapping field approach was considered to alleviate the block effect within the restored image.

Moreover, a depth variant maximum likelihood restoration approach was developed in (Preza and Conchello [2004]) to compensate for degradation changing with depth in 3D fluorescence microscopy images. In that method, C. Preza and J. Conchello propose a decomposition of the 3D image into strata along the optical axis, where the PSF is considered as variant. They associate to each stratum a space-invariant PSF which is estimated as a weighted interpolation between the PSF at the top and at the bottom of the considered stratum.

Object estimation is then achieved using maximum likelihood expectation-maximization algorithm embedded with the proposed PSF modeling.

Recently, an evolutionary merging mask algorithm (EMMA) was introduced in (Maalouf [2010]) for 3D fluorescence microscopy images. It consists in separately performing multiple deconvolution with different space-invariant PSF on the whole image, using any classical deconvolution algorithm, the PSF at different few depths is assumed to be known. The deconvolved images are then merged together using an adequate mask that takes the best of each part to build the final estimated object.

Finally, we cite a new method recently proposed in (Hajlaoui et al. [2010]) for restoration of satellite images (captured with push broom sensors) that suffer from a variant blur along the orthogonal direction of the satellite motion. It mainly consists in fitting the forward-backward algorithm to the case of block-varying PSF using wavelet frame regularization.

In spite of local-invariance approximation of the PSF, most of these listed methods remain computationally intensive due to their iterative and sequential formulation. In our work, we propose a fast restoration approach for space-varying blurred images, where the true image estimation can be performed in a parallel way in different sub-domains of the image, thanks to an image decomposition strategy. We first introduce an image observation model that takes into account space blur-variation. We consider a blur modeled by a space-varying linear combination of spatially invariant blurs. In particular, we consider a piecewise-constant PSF with regular transition between zones in order to reduce mosaic effect of the block decomposition. Secondly, we deal with the inversion problem of such a model by minimizing a criterion

including a total variation regularization. We rely on an energy optimization method based on a domain decomposition strategy that was recently developed in (Fornasier et al. [2009]). The main advantage of this method is that energy minimization is processed in a parallel way on different areas of the image while taking into account the estimates in the adjacent areas of the considered sub-image. Furthermore, we check the validity of some criteria in the case of space-varying PSF model in order to do not break the convergence properties of the proposed optimization method.

This report is organized as follows: in the second section, we present the proposed approximate observation model for space-varying blurred image. In the third section, we explicit the associated deconvolution approach which is mainly based on the optimization method proposed by Fornasier et al. In particular, we show how we fitted such a method to the proposed space-varying PSF model and we study its convergence properties. In the fourth section, we report and evaluate some numerical results obtained on a 2D synthetic image as well as a simulated 3D biological image. Finally, we conclude this report by proposing some perspectives which could complete our research work.

2 Space-varying PSF model

Before presenting the image formation model that we deal with, let us collect the main notations used in this report.

2.1 Notations

As the observation is usually done with a matrix of CCD sensors, we consider discrete notations. Let $\Omega = \left\{x_1^1, \ldots, x_{N_1}^1\right\} \times \ldots \times \left\{x_1^d, \ldots, x_{N_d}^d\right\} \subset \mathbb{R}^{N_1 \times \ldots \times N_d}$, $d = 1, 2, 3$ be the image dimension, Ω the image domain, and let $\mathcal{F}$ be the space of functions from Ω to $\mathbb{R}$ standing for one pixel intensity. We denote by $\mathcal{H} = \mathbb{R}^{N_1 \times \ldots \times N_d}$, the space of vectors that refers to the whole image intensity. A vector u in $\mathcal{H}$ can be written as $u = (u(x))_{x \in \Omega}$. We endow $\mathcal{H}$ with the following norms:

- $\| u \|_p = \left(\sum_{x \in \Omega} | u(x) |^p \right)^{1/p}$; $\forall u \in \mathcal{H}$, $1 \leq p < \infty$,
- $\| u \|_\infty = \max_{x \in \Omega} | u(x) |$; $\forall u \in \mathcal{H}$.

We define the scalar product of $u, v \in \mathcal{H}$ as follows:

$$< u, v > = \sum_{x \in \Omega} u(x) . v(x)$$

Moreover, we denote by $\mathcal{L}$ the space of linear operators $H : \mathcal{H} \longrightarrow \mathcal{H}$ and we associate it with the following norm:

- $$\| H \|_p = \max_{u \in \mathcal{H} \setminus \{0\}} \frac{\| H(u) \|_p}{\| u \|_p}$$
$$= max \{ \| H(u) \|_p \; such \, that \; \| u \|_p \leq 1 \}.$$

We also introduce the space $\mathcal{P} = \mathcal{H}^d$ such that any p in $\mathcal{P}$ can be written as $p = (p_i)_{1 \leq i \leq d}$. Furthermore, for any $p \in \mathcal{P}$ and any $x \in \Omega$, we define $|p(x)|_\infty = max \{ |p_i(x)|, 1 \leq i \leq d \}$. We thus introduce the following closed convex set which will be used later for the computation of the restored image using total variation regularization:

$$K = \{ div \, p : \; p \in \mathcal{P} \, such \, that \, |p(x)|_\infty \leq 1, \; for \, all \, x \in \Omega \} \tag{3}$$

where *div* stands for the divergence operator.

2.2 Space-varying blur modeling

In order to take into account the blur variation of the optical distorting system, we consider a blur modeled by a space-varying linear combination of spatially invariant blurs. Denoting by $g \in \mathcal{H}$ the blurred image, $u \in \mathcal{H}$ the original one, and $\{h_i, 1 \leq i \leq D\}$ a finite set of space-invariant PSF, an approximation of the image formation process is given by the following equation:

$$g(x) = \sum_{1 \leq i \leq D} \psi_i(x) \,.\, (h_i * u)(x), \forall x \in \Omega \tag{4}$$

where $*$ stands for the discrete circular convolution and ψ_i are weighting functions in $\mathcal{H}$.

In particular, we consider a piecewise-constant PSF model with regular transition between zones. In fact, we assume that regions where the blur-variation is negligible are affected by the same constant blur. To build the image observation model, we propose to split the domain Ω into D overlapping sub-domains as it was initially proposed in (Fornasier et al. [2009]). In other words, we consider that the image domain Ω is sectioned into a set of sub-domains $\{\Omega_i \subset \Omega, 1 \leq i \leq D\}$ such that adjacent sub-domains are overlapping i.e. $\Omega = \underset{1 \leq i \leq N}{\cup} \Omega_i$ such that $\Omega_i \cap \Omega_{i+1} \neq \emptyset$. An example of such a domain decomposition into two overlapping sub-domains is displayed in Fig. 1. We assume that each block is affected by a space-invariant blur represented by a given PSF h_i, $1 \leq i \leq D$. In addition, blur alteration from one block to another is not done in a brutal way but it is allayed by introducing weighting functions $\psi_i \in \mathcal{H}$ with $support(\psi_i) = \Omega_i$ for $1 \leq i \leq D$. These functions allow to smooth PSF variation between zones where Ω_i and Ω_{i+1} overlap. Some additional constraints on the map set $\{\psi_i, 1 \leq i \leq D\}$, similar to those proposed in (Fornasier et al. [2009]), are introduced in order to preserve the convergence properties of the proposed restoration method. The functions ψ_i, $1 \leq i \leq D$ must satisfy the following conditions:

1. $0 \leq \psi_i \leq 1$, for $1 \leq i \leq D$,
2. $\sum_{i=1}^{D} \psi_i(x) = 1, \forall x \in \Omega$.

For ease of presentation, we consider a space decomposition into two domains. Furthermore, we propose to use in our later work a classical example of weighting functions ψ_1 and ψ_2 as that displayed in Fig. 2. In this case, the observation model given by (4) can be written as follows:

$$g(x) = \begin{cases} (h_1 * u)(x) & if\ x \in \Omega_1 \setminus \Omega_2 \\ \psi_1(x).(h_1 * u)(x) + \psi_2(x).(h_2 * u)(x) & if\ x \in \Omega_1 \cap \Omega_2 \\ (h_2 * u)(x) & if\ x \in \Omega_2 \setminus \Omega_1 \end{cases}$$

Note that the above equation represents a particular case of the proposed observation model given by (4) which was constrained by the choice of particular weighting functions. Actually, the proposed restoration method that we will describe in the following section remains valid for any other choice of the weighting functions as long as they verify the two previous conditions. Thanks to such a modeling, we obtain a PSF which is different at each point of the image domain. We can illustrate this idea by developing the equation corresponding to the image formation model when considering, for example, two PSF:

$$\begin{aligned} g(x) &= \psi_1(x).(h_1 * u)(x) + \psi_2(x).(h_2 * u)(x) \\ &= \psi_1(x).\left(\sum_t h_1(x-t).u(t)\right) + \psi_2(x).\left(\sum_t h_2(x-t).u(t)\right) \\ &= \sum_t \left[\psi_1(x).h_1(x-t) + \psi_2(x).h_2(x-t)\right].u(t) \\ &= \sum_t h(x,t).u(t) \end{aligned}$$

with $h(x,t) = \psi_1(x).h_1(x-t) + \psi_2(x).h_2(x-t)$.

Hence, considering such a model leads to a space-variant filtering. Indeed, because of the introduction of transition functions, the blur function $h(x,.)$ changes at every point x of the image. That's why, we introduced the operator $\widetilde{H} \in \mathcal{L}$ which indicates the non-stationary convolution with the proposed PSF model. To be more precise, we denote by $\widetilde{H}$ the operator given by the following equation:

$$\widetilde{H}(.) = \psi_1.H_1(.) + \psi_2 H_2(.) \tag{5}$$

where $H_1(.) = h_1 *.$ denotes the circular convolution operator with the space-invariant PSF h_1 and $H_2(.) = h_2 * .$ corresponds to the circular convolution operator with the space-invariant PSF h_2. Let remark that computing $\widetilde{H}(u)$ can be rapidly done by making the convolutions by H_1 and H_2 in the Fourier domain and then the linear combination in the spatial domain for each $x \in \Omega$.

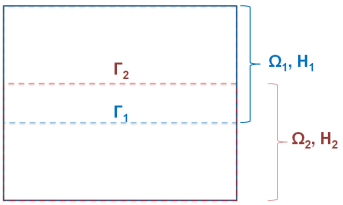

Figure 1: Overlapping domain decomposition into two sub-domains

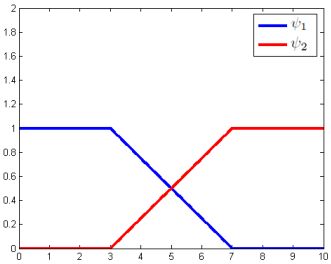

Figure 2: Weighting functions $\psi_1(.)$ and $\psi_2(.)$ for two overlapping domain decomposition.

3 Image restoration method within a framework of a space-varying PSF

After defining the image formation model, we now interest on inverting the space-varying PSF by minimizing an energy functional formed by a quadratic term corresponding to data fidelity and a total variation regularization (Rudin et al. [1992], Rudin and Osher [1994], Chambolle and Lions [1997]). The main role of the total variation term is that it allows the smoothness of homogeneous areas while preserving edges. We stress that it is important to take into account such a term during the deconvolution process since inversion with a low-pass filter such as the PSF amplifies high frequencies and then amplifies the noise even if it is small. We thus consider the following functional to be minimized w.r.t. $u \in \mathcal{H}$:

$$J(u) = \left\| \widetilde{H}(u) - g \right\|_2^2 + 2\alpha \|\nabla u\|_1 \tag{6}$$

where $\alpha > 0$ is a fixed regularization parameter. In order to minimize such a functional, we are interested in an efficient optimization method that was recently developed in (Fornasier et al. [2009]). It was studied for a constant linear operator. Its convergence was theoretically proved under some conditions. Moreover, it was successfully applied on signal interpolation and 2D image inpainting. It also showed promising results in terms of computational time. In this section, we propose to summarize the underlying principles of this method and fit it to the problem of decovolution with a space-varying PSF according to the proposed model. Furthermore, we check the validity of some properties related to the convergence of this procedure when considering the proposed non-stationary convolution.

3.1 Overlapping domain strategy for energy minimization

We detail here the alternating subspace minimization algorithm described in (Fornasier et al. [2009]), for the non-stationary convolution operator $\widetilde{H}(.)$. First of all, we should stress that the minimization approach proposed in (Fornasier et al. [2009]) was carried out in a discrete approximation framework and a discrete expression of the energy function (6) was introduced. In fact, the solution proposed by Fornasier et al. consists in instead of minimizing the functional (6) on the whole domain Ω to minimize it in a parallel way on sub-domains of Ω using a domain decomposition strategy, in order to reduce the computational time. An overlapping domain splitting similar

to that described in the previous section was proposed. In that method, the sub-domains Ω_i, $1 \leq i \leq N$ are subject to a constraint given by a splitting property of the total variation term (equation 2, (Fornasier et al. [2009])). Note that the number of sub-domains N considered in the minimization method is not necessarily the same as that chosen in the PSF modeling and one can choose a domain decomposition different from that proposed in the previous section. For sake of clarity, we also present this method for two sub-domains Ω_1 and Ω_2 (cf. Fig. 1). However, the method is easily generalizable to multiple domains. Considering such a domain splitting, a possible decomposition of the solution $u \in \mathcal{H}$ of the minimization problem of function (6) is given by:

$$u(x) = \begin{cases} u_1(x) & if\, x \in \Omega_1 \setminus \Omega_2 \\ u_1(x) + u_2(x) & if\, x \in \Omega_1 \cap \Omega_2 \\ u_2(x) & if\, x \in \Omega_2 \setminus \Omega_2 \end{cases} \tag{7}$$

where function u_i is in the subspace $V_i = \{u \in \mathcal{H},\, support\,(u) \subset \Omega_i\}$, for $i \in \{1, 2\}$. Moreover, we denote by Γ_1 the interface between Ω_1 and $\Omega_2 \setminus \Omega_1$ and by Γ_2 the interface between Ω_2 and $\Omega_1 \setminus \Omega_2$ (cf. Fig. 1). With this splitting, Fornasier et al. propose to perform the minimization of functional (6) in each sub-domain taking into account the estimates in the other sub-domains. Let consider, for instance, the following minimization problem on the sub-domain Ω_1:

$$u_1^* = Arg \underset{u_1 \in V_1 / Tr|_{\Gamma_1} u_1 = 0}{Min} J(u_1 + u_2) \tag{8}$$

where $Tr|_{\Gamma_1} u_1 = u_1|_{\Gamma_1}$ is the restriction of u_1 on the boundary Γ_1. The main difficulty of the proposed subspace minimization method is finding an appropriate algorithm for solving the problem of local minimization of functional $J(.)$ w.r.t. u_1 given by (8) while preserving the condition $Tr|_{\Gamma_1} u_1 = 0$. Indeed, because of such a condition, classical minimization methods based on gradient descent scheme are no directly applicable. For that matter, Fornasier et al. propose to use a *Lagrange multiplier* scheme. The main idea of this algorithm is minimizing an auxiliary function of $J(.)$ where the variable u_1 is not affected by the action of the blur operator $\widetilde{H}$. An algorithmic solution of such a minimization problem is then accessible using an *oblique thresholding* theorem which will be presented afterwards. Now, let detail the proposed Lagrange multiplier scheme (Fornasier et al. [2009]) for local minimization. It consists in minimizing an auxiliary functional $J_1^s(.)$ of $J(.)$

called *surrogate functional* (Fornasier and Schönlieb [2009], Fornasier et al. [2009]) of $J(.)$ by iterating the following equation:

$$u_1^{(l+1)} = Arg \underset{u_1 \in V_1/Tr|_{\Gamma_1} u_1 = 0}{Min} J_1^s \left(u_1 + u_2,\, u_1^{(l)} \right),\ l \geq 0 \tag{9}$$

where $J_1^s(.)$ is defined as follows:
$J_1^s \left(u_1 + u_2,\, u_1^{(l)} \right) = J(u_1 + u_2) + \left\| u_1 - u_1^{(l)} \right\|_2^2 - \left\| \widetilde{H} \left(u_1 - u_1^{(l)} \right) \right\|_2^2$
with $u_1,\, u_1^{(l)} \in V_1,\, u_2 \in V_2$. We can rewrite $J_1^s \left(u_1 + u_2,\, u_1^{(l)} \right)$ in the following form such that the variable u_1 is not anymore affected by the action of $\widetilde{H}(.)$:

$$J_1^s \left(u_1 + u_2,\, u_1^{(l)} \right) = \|u_1 - z_1\|_2^2 + 2\alpha \left\| \nabla (u_1 + u_2) \,|\, (\Omega_1) \right\|_1 \tag{10}$$

with $z_1 = u_1^{(l)} + \left(\widetilde{H}^* \left(g - \widetilde{H}(u_2) - \widetilde{H} \left(u_1^{(l)} \right) \right) \right) \,|\, \Omega_1$ where $\widetilde{H}^*(.)$ denotes the adjoint of the non-stationary convolution operator $\widetilde{H}(.)$. Thus, we look for an expression of the adjoint $\widetilde{H}^*(.)$. Let $u, v \in \mathcal{H}$,

$$< \widetilde{H}(u), v > \ = \ < \psi_1 . H_1(u), v > + < \psi_2 . H_2(u), v >$$

We focus on developing the first part of the second term of the above equation:

$$\begin{aligned} < \psi_1 . H_1(u), v > &= \sum_{x \in \Omega} \psi_1(x) . (h_1 * u)(x) . v(x) \\ &= \sum_{x \in \Omega} (h_1 * u)(x) . \psi_1(x) . v(x) \\ &= < H_1(u), \psi_1 . v > \\ &= < u, H_1^*(\psi_1 . v) > \end{aligned}$$

Thus, $< \widetilde{H}(u), v > = < u, H_1^*(\psi_1 . v) + H_2^*(\psi_2 . v) >$. That is to say, $\widetilde{H}^*(v) = H_1^*(\psi_1 . v) + H_2^*(\psi_2 . v)$, where $H_1^*(.)$ and $H_2^*(.)$ are respectively adjoints of $H_1(.)$ and $H_2(.)$. Let remark that the adjoint operator $\widetilde{H}^*$ can also be computed by multiplication in the Fourier domain (for H_1^* and H_2^* convolutions) after multiplying v by ψ_1 and ψ_2. Then, the computation of the adjoint operator is also fast. In order to provide an algorithmic solution of the local minimization problem, the following *oblique thresholding* theorem was used in (Fornasier et al. [2009]).

Theorem 1. *The following two statements are equivalent:*

1. $u_1^* = Arg \underset{u_1 \in V_1/Tr|_{\Gamma_1} u_1 = 0}{Min} \|u_1 - z_1\|_2^2 + 2\alpha \left\| \nabla (u_1 + u_2) \,|\, (\Omega_1) \right\|_1$,

2. $\exists\, \eta \in V_1$ *with* $support\,(\eta) = \Gamma_1$ *such that:*

$$u_1^* = (I - P_{\alpha K})\,(z_1 + u_2 - \eta) - u_2 \; and \; Tr|_{\Gamma_1} u_1^* = 0 \tag{11}$$

where $P_{\alpha \mathrm{K}}\,(u) = Arg\,\underset{v \in K}{Min}\,\|u - v\|_2$, *for* $u \in \mathcal{H}$ *is the orthogonal projection onto the closed convex set* K *given by (3).*

Numerical computation of the orthogonal projection can be performed thanks to the dual method of Chambolle (Chambolle [2004]). The proof of such a theorem is provided in (Fornasier et al. [2009]).

In addition, it is shown in (Fornasier et al. [2009]) that $\eta \in V_1$ as in statement 2 of the previous theorem is a fixed point of the following equation:

$$\eta = (Tr|_{\Gamma_1})^*\, Tr|_{\Gamma_1}\,(z_1 + P_{\alpha K}\,(\eta - (z_1 + u_2))) \tag{12}$$

and it is accessible by means of the following iterative algorithm:

Algorithm 1 Fixed point computation

- Initialize $\eta^{(0)} \in V_1$, $support\,(\eta) = \Gamma_1$
- For m from 0 to $(M-1)$, iterate the following equation:

$$\eta^{(m+1)} = (Tr|_{\Gamma_1})^*\, Tr|_{\Gamma_1}\left(z_1 + P_{\alpha K}\left(\eta^{(m)} - (z_1 + u_2)\right)\right)$$

The convergence of the above algorithm to a fixed point of function given by (12) was shown in (Fornasier et al. [2009]) using the strong non-expansive property of the projection $P_{\alpha K}$ (Bauschke et al.). This latter do not depend on the non-stationary convolution operator $\widetilde{H}\,(.)$, but only on the convex set K due to the regularization term. Hence, this property still holds in the case that we are dealing with. Thus, by computing η and including it in (11), the local minimization problem of function $J_1^s\,(.)$ given by (10) is solved and a partial value of the image u on the sub-domain Ω_1 is obtained. The global minimization algorithm of functional (6) that allows for the computation of the solution u on the whole domain Ω consists in alternating subspace minimization using (8) and its symmetrical for the computation of u_2 and then combining the obtained local solutions using (7). In (Fornasier et al. [2009]), two versions of the global minimization algorithm are presented, i.e. the sequential and the parallel algorithms. We choose here to focus on the parallel algorithm where local minimizations are simultaneously performed

as it is more interesting in terms of computational time. It is expressed as follows:

Algorithm 2 Parallel version of the alternating subspace minimization algorithm

- Initialize $u^{(0)} = \tilde{u}_1^{(0)} + \tilde{u}_2^{(0)}$, $\left(e.g.\ \tilde{u}_1^{(0)} = 0,\ \tilde{u}_2^{(0)} = 0\right)$
- Initialize the number of iterations N, L and I,
- Initialize the regularizing parameter α,
- For n from 0 to $(N-1)$, iterate the following steps:

  Step 1: Energy minimization on the sub-domain Ω_1

  - Initialize $u_1^{(n+1,0)} = \tilde{u}_1^{(n)}$,
  - For l from 0 to $(L-1)$, iterate the following equation:

$$u_1^{(n+1,l+1)} = Arg \underset{u_1 \in V_1 / Tr|_{\Gamma_1} u_1 = 0}{Min} J_1^s \left(u_1 + \tilde{u}_2^{(n)}, u_1^{(n+1,l)}\right)$$

  Step 2: Energy minimization on the sub-domain Ω_2

  - Initialize $u_2^{(n+1,0)} = \tilde{u}_2^{(n)}$
  - For i from 0 to $(I-1)$, iterate the following equation:

$$u_2^{(n+1,i+1)} = Arg \underset{u_2 \in V_2 / Tr|_{\Gamma_2} u_2 = 0}{Min} J_2^s \left(\tilde{u}_1^{(n)} + u_2, u_2^{(n+1,i)}\right)$$

  Step 3: $u^{(n+1)} = \dfrac{u_1^{(n+1,L)} + u_2^{(n+1,I)} + u^{(n)}}{2}$

  Step 4: $\begin{cases} \tilde{u}_1^{(n+1)} = \chi_1 . u_1^{(n+1)} \\ \tilde{u}_2^{(n+1)} = \chi_2 . u_2^{(n+1)} \end{cases}$

$\{\chi_1, \chi_2\} \subset \mathcal{H}$ is a bounded uniform partition of unity (BUPU) that satisfies the following conditions:

1. $Tr|_{\Gamma_i} \chi_i = 0$ for $i = 1, 2$,
2. $\chi_1 + \chi_2 = 1$,

3. $support\,(\chi_i) \subset \Omega_i$ for $i = 1,\, 2$,

4. $Max\,\{\|\chi_1\|_\infty\,,\, \|\chi_2\|_\infty\} < \infty$.

The main role of these functions $\{\chi_1, \chi_2\} \subset \mathcal{H}$ is to ensure the boundedness of the sequences $\left(\widetilde{u}_1^{(n)}\right)_{n\in\mathbb{N}}$ and $\left(\widetilde{u}_2^{(n)}\right)_{n\in\mathbb{N}}$ produced by the previous algorithm and thus prove the existence of an optimal decomposition $u^{(\infty)} = \tilde{u}_1^{(\infty)} + \tilde{u}_2^{(\infty)}$ used in the convergence proof of the proposed minimization method. A classical example of these auxiliary functions χ_1 and χ_2 is presented in Fig. 2. Furthermore, the main advantage of the overlapping sub-domains property proposed in (Fornasier et al. [2009]) is simplifying the theoretical proof of the convergence of the global minimization algorithm by avoiding a fine analysis on the interfaces Γ_1 and Γ_2. Moreover, the number of iterations N, L and I are manually set to high values in order to achieve the global optimum of the energy function. Nevertheless, one can use a stopping criterion for the iterative algorithm. For instance, the convergence of such an iterative algorithm is usually assumed to be reached when the vector u remains stable during iterations. That is to say, the mean square error, for example, between two successive outputs ($u^{(n)}$ and $u^{(n+1)}$) is below a very low fixed threshold. In addition, further constraints on the operator $\widetilde{H}\,(.)$ are required in order to ensure the convergence of the proposed minimization method to an optimal solution. This issue will be the subject of the following sub-section.

3.2 Convergence of the proposed energy minimization method

After describing the alternating subspace minimization algorithm fitted to the proposed non-stationary convolution operator, we now interest in proving its convergence. From the convergence proof established in (Fornasier et al. [2009]) for space-invariant linear operator, we exhibit two necessary conditions. First, the operator $\widetilde{H}\,(.)$ should allow the coercivity of the functional $J\,(.)$ given by (6). In fact, if J is coercive in $\mathcal{H}$ then there exists a constant $C > 0$ such that $\{u \in \mathcal{H} : J\,(u) \leq C\}$ is bounded in $\mathcal{H}$. That is to say, there exists a subsequence of the sequence $\left(u^{(n)}\right)_{n\in\mathbb{N}}$ produced by the algorithm which converges to a finite limit $u^{(\infty)}$. We thus introduce the definition of a coercive function.

Definition 2. *$J\,(.)$ is called coercive if: $J\,(u) \to +\infty$ as $\|u\| \to +\infty$.*

To prove such a property, it suffices to show that $1 \notin Ker\left(\widetilde{H}\right)$, where $Ker\left(\widetilde{H}\right) = \left\{u \in \mathcal{H} :\ \widetilde{H}(u) = 0\right\}$. Indeed,

$$\widetilde{H}(1)(x) = \sum_t \left(\psi_1(x).h_1(x-t) + \psi_2(x).h_2(x-t)\right) \tag{13}$$

Since we deal with normalized and positive PSF i.e. $\|h_i\|_1 = \sum_t |h_i(t)| = \sum_t h_i(t) = 1$ for $i \in \{1, 2\}$, the previous equation (13) can be expressed as:

$$\widetilde{H}(1)(x) = \psi_1(x) + \psi_2(x) = 1 \tag{14}$$

and therewith finishes the proof.

A second necessary condition for the convergence of the proposed minimization method is $\left\|\widetilde{H}\right\|_2 \leq 1$. It contributes to certain convergence properties of the sequence $\left(u^{(n)}\right)_{n\in\mathbb{N}}$ such as:

1. $J\left(u^{(n)}\right) > J\left(u^{(n+1)}\right),\ \forall n \in \mathbb{N}$ unless $u^{(n)} = u^{(n+1)}$
2. $\lim_{n\to\infty} \left\|u^{(n+1)} - u^{(n)}\right\|_2 = 0.$

We can easily prove that for any stationary convolution operator $H(.) = h*.$, we have $\|H\|_2 \leq 1$ if h is normalized i.e. $\|h\|_1 = 1$. Furthermore, using the properties of the circulant matrix corresponding to a space-invariant PSF, we can also prove that $\|H\|_2 \leq \frac{1}{\sqrt{n}}$ with $n = Card(\Omega)$. In fact, it is known that any circulant matrix is diagonalizable with normalized discrete Fourier transform. Thus, $\| H \|_2$ is bounded by the maximal eigenvalue of that matrix which itself is bounded by $\frac{1}{\sqrt{n}}$ since this eigenvalue is computed as a normalized discrete Fourier transform of the PSF in the zero coordinate. Now, let prove the validity of this condition for space-varying operator (i.e. $\| \widetilde{H} \|_2 \leq 1$). We define the following norm corresponding to $\widetilde{H}$:

$$\| \widetilde{H} \|_2 = max\left\{\| \widetilde{H}(u) \|_2 \ such\, that \ \| u \|_2 \leq 1\right\} \tag{15}$$

Let u be in $\mathcal{H}$ such that $\|u\|_2 \leq 1$. It is easy to verify that:

$$\| \widetilde{H}(u) \|_2 \leq \sqrt{n} \| \widetilde{H}(u) \|_\infty . \tag{16}$$

It suffices to show that $\| \widetilde{H}(u) \|_\infty \leq \frac{1}{\sqrt{n}}$.

We have $\| \widetilde{H}(u) \|_\infty = \max_{x\in\Omega} | \left[\widetilde{H}(u)\right](x) |$ which means that $\| \widetilde{H}(u) \|_\infty = \max_{x\in\Omega} | \psi_1(x).H_1(u)(x) + \psi_2(x).H_2(u)(x) |$.

Using the triangle inequality, we obtain:

$$\| \widetilde{H}(u) \|_\infty \leq \max_{x\in\Omega} |\psi_1(x)|.|H_1(u)(x)| + |\psi_2(x)|.|H_2(u)(x)| \tag{17}$$

Besides, we know that for a stationary operator $H_i, i = 1, 2$, we have $\|H_i\|_2 \leq \frac{1}{\sqrt{n}}$ which implies that $\|H_i\|_\infty \leq \frac{1}{\sqrt{n}}$ since $\|H_i\|_\infty \leq \|H_i\|_2$. Hence, we deduce that:

$|H_1(u)(x)| \leq \frac{1}{\sqrt{n}}$, *and* $|H_2(u)(x)| \leq \frac{1}{\sqrt{n}}$, $\forall x \in \Omega$. Taking into account this last conclusion in (17), we obtain:

$$\| \widetilde{H}(u) \|_\infty \leq \frac{1}{\sqrt{n}} \max_{x\in\Omega} |\psi_1(x)| + |\psi_2(x)| \tag{18}$$

Consequently, by combining (16) and (18), we find:

$$\| \widetilde{H}(u) \|_2 \leq \sqrt{n} \| \widetilde{H}(u) \|_\infty \leq \max_{x\in\Omega} |\psi_1(x)| + |\psi_2(x)| \tag{19}$$

Thereby, we proved that $\| \widetilde{H} \|_2 \leq 1$ as $|\psi_1(x)| + |\psi_2(x)| = 1$, $\forall x \in \Omega$.

With this property validation, the rest of the convergence proof follows analogous arguments as that in (Fornasier et al. [2009]).

4 Numerical results

In this section, we provide some numerical experiments in order to assess the presented restoration method and illustrate the advantage of the space-variance approach. We interest in two particular examples. The first test was performed on a 2D synthetic image distorted with a variant blur according to the presented observation model. This allows us to validate our restoration approach since the considered image follows exactly the considered blur modeling (there is no any approximation included in the image observation model). We also evaluate the robustness of our method against noise and we consider a space-varying blurred image corrupted with an additive white Gaussian noise. Moreover, to assess the quality of our restoration algorithm, we provide some numerical measures such as the mean square error and the peak signal-to-noise ratio. Secondly, we test the proposed method on a simulated 3D image of a fluorescence confocal microscopy, the blur is continuously varying along the optical direction.

4.1 Test on a 2D synthetic image

First, we consider the 2D synthetic image of 128×128 pixels displayed in Fig. 3(a). We blurred this image with four different Gaussian PSF, each corresponds to a given region. We thus consider an overlapping domain decomposition into four sub-domains. Its interfaces are depicted in Fig. 3(e), The red line corresponds to the lower side of the first rectangular sub-domain Ω_1, the two green lines correspond to the interfaces of the sub-domain Ω_2, the blue ones correspond to those of the third sub-domain Ω_3 and the yellow line represent the upper side of the sub-domain Ω_4. Weighting functions as those displayed in Fig. 2 are considered in the proposed distortion modeling. The considered PSF have a zero mean and respectively the following standard deviations $\sigma_1 = 1$, $\sigma_2 = 1,75$, $\sigma_3 = 2,5$ and $\sigma_4 = 3,25$. The resulting distorted images is depicted in Fig. 3(b). The restored image displayed in Fig. 3(c) shows the relevance of the proposed deblurring method. Note that the reconstruction method was performed by considering the same decomposition as that used for the generation of the blurred image. The regularizing parameter is fixed to $\alpha = 10^{-4}$. The evolution of the energy functional during iterations is plotted in Fig. 4(a). Actually, it illustrates the convergence of the estimation method. In this test, the numbers of iterations of local and global minimization algorithms are respectively set to 30 and 60. But one can notice from the curve of the energy functional depicted in Fig. 4(a) that 20 iterations of the global algorithm are sufficient to reach the optimum of the energy function. The simulation of the algorithm on a machine having a multi-core processor (8 cores) of a frequency 1.86 GHz required only $1\,mn\,and\,20\,s$ to reach its convergence. In fact, the method was programmed in Matlab and the code is not optimized. The computing time can be reduced by optimizing the code using the C++ programming language for example. Furthermore, knowing the true image value, we compute the mean square error (MSE) between the estimated object and the true one using the following formula in order to assess the accuracy of our estimation method.

$$MSE\left(u,o\right) = \frac{1}{Card\left(\Omega\right)} \sum_{x \in \Omega} \left(u\left(x\right) - o\left(x\right)\right)^2 \tag{20}$$

with $u\left(.\right)$ is the estimated object and $o\left(.\right)$ is the original one, before degradations. The plot of the MSE versus iterations is presented in Fig. 4(b). It illustrates the fast convergence of our algorithm. In order to highlight the advantage of the space-variance approach, we also restored the image using a single PSF having a zero mean and a standard deviation equals the mean of the four standard deviation of the four PSF used for the image degradation

($\sigma = 2,125$). One can notice a poor restoration especially in the higher and lower regions of the restored image of Fig. 3(d).

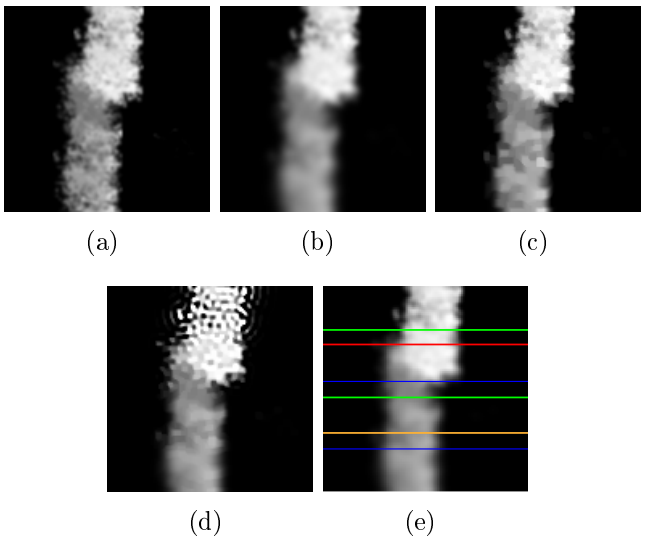

(a) (b) (c)

(d) (e)

Figure 3: (a) Original image, (b) blurred image with four Gaussian PSF, (c) restored image with the space-variance approach, (d) restored image with space invariance assumption, (e) interfaces of the considered domain decomposition.

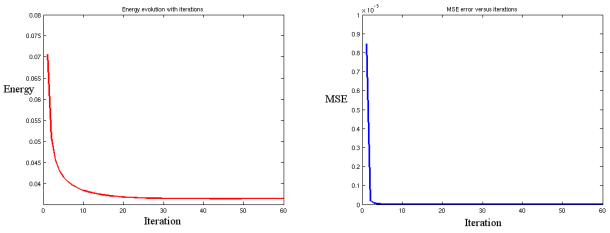

(a) (b)

Figure 4: (a) Energy evolution with iterations and (b) mean square error versus iterations corresponding to the proposed restoration procedure with space-varying PSF.

Second, in order to evaluate the robustness of our method against noise, we test it on an image of 256×256 pixels affected by the same blur functions as those considered in the previous test (four Gaussian PSF) and corrupted with an additive Gaussian noise having a standard deviation equals $\sigma = 9$. The images before and after degradations are respectively depicted in Fig.

5(a) and Fig. 5(b). Similar parameter values (number of iterations of local and global algorithms) as those chosen in the previous test, are considered. The regularizing parameter is set to $\alpha = 5\,.\,10^{-3}$. The computing time is about $2\,mn$. The restored image as well as the image corresponding to the difference between this latter and the original image are respectively displayed in Fig. 5(c) and Fig. 5(d). We also present in Fig. 5(e) and Fig. 5(f) those obtained when considering one Gaussian PSF of zero mean and standard deviation $\sigma = 2,125$. Visually, we can notice in Fig. 5(c) a good restoration for the considered noisy image. In fact, the restored image with the space variance approach is very close to the real one (cf. Fig. 5(d)). However, the restored image with one invariant PSF is well denoised but not well deblurred. In addition, we numerically evaluate the robustness of the restoration method against noise and we compute the peak signal-to-noise ratio using the following formula $PSNR = 10\,log_{10}\dfrac{D^2}{MSE\,(g,u)}$ with D the dynamic range of the image intensity. It is about $24\,dB$.

4.2 Test on a simulated 3D biological image

We interest now in testing our algorithm on a 3D image assumed to be acquired with a confocal laser scanning microscope (CLSM) (Minsky [1988], Inoué [2006]). The main particularity of such a system is that it distorts the image with a depth-varying blur. It is mainly due to the refraction phenomenon because of the variation of the refractive index in the system as well as aberrations due to the increasing imaging depth. Ideally, the first plane immediately below the coverslip is free of aberrations. In this test, we consider a simulated CLSM image of two micro-spheres placed at two different depths. The actual object is thus exactly known. Hence, an effective evaluation of the proposed method can also be obtained by comparing the estimated object w.r.t the true one. In what follows, we describe the imaging conditions with the considered acquisition parameters that we used for the PSF generation. Then, we present and discuss the obtained results.

4.2.1 Simulating the observation

We generated two spherical beads having each a diameter of 672 nm in a volume of 9648 nm $\times$ 9648 nm $\times$ 4848 nm. The first bead is placed at a depth of 1440 nm along the optical axis and the second bead is placed at a depth of 3360 nm. These micro-spheres are supposed to be embedded in a medium of a refractive index $n_s = 1.45$. Fig. 7(a) displays the simulated original object. This object is assumed to be imaged by a CLSM system having a

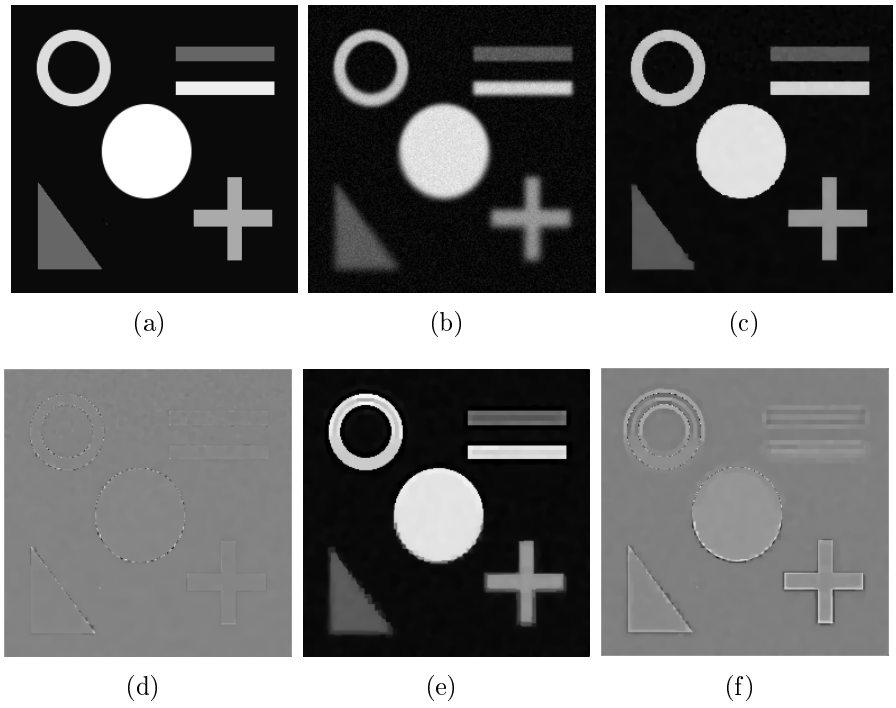

Figure 5: (a) Original image, (b) blurred and noisy image, (c) restored image with the space variance approach, (d) intensity difference between the restored and original images, (e) restored image with space invariance assumption, and (f) intensity difference between the restored and original images.

magnification of $100X$, a numerical aperture of NA=1.4 and an oil immersed lens with a refractive of $n_i = 1.5$. The coverslip chosen has a refractive index very close to that of the objective medium, so that aberration induced by the mismatch of the refractive index between these two mediums is negligible. The excitation and emission peaks are respectively at wavelengths of 543 nm and 600 nm. The pinhole of the confocal microscope is adjusted to a very small physical size so that it can be approximated by a Dirac function in the PSF equation (Stokseth [1969], Pankajakshan et al. [2009]). Furthermore, the image reconstruction respects the Nyquist sampling, the lateral and the axial pixel sizes are set to 48 nm. Knowing all the imaging setup conditions, the PSF can be computed using a mathematical PSF model based on the Stokseth approximation (Stokseth [1969], Pankajakshan et al. [2009]). Fig. 6 displays the maximum intensity projection of the simulated PSF onto the lateral and the axial planes for two different depths. Fig. 6(a) and Fig. 6(c) correspond to a PSF for a zero depth under the coverslip and Fig. 6(b) and

Fig. 6(d) correspond to a PSF generated at a depth of 4800 *nm*. One can see the axial shift of the PSF measured at a deep point under the coverslip w.r.t. that generated at a zero depth. However, the radial PSF is practically unchangeable with depth (cf. Fig. 6(a) and Fig. 6(b)). This illustrates the PSF variation along the axial direction for CLSM images discussed at the beginning of this section. Since the PSF is different for each z-slice, we generated 101 PSF, each of them corresponds to a z-slice. An accurate simulation of axially-variant blurred CLSM image is then obtained by performing 101 convolutions with the appropriate PSF. Axial slice of the obtained distorted image is displayed in Figure 7(b).

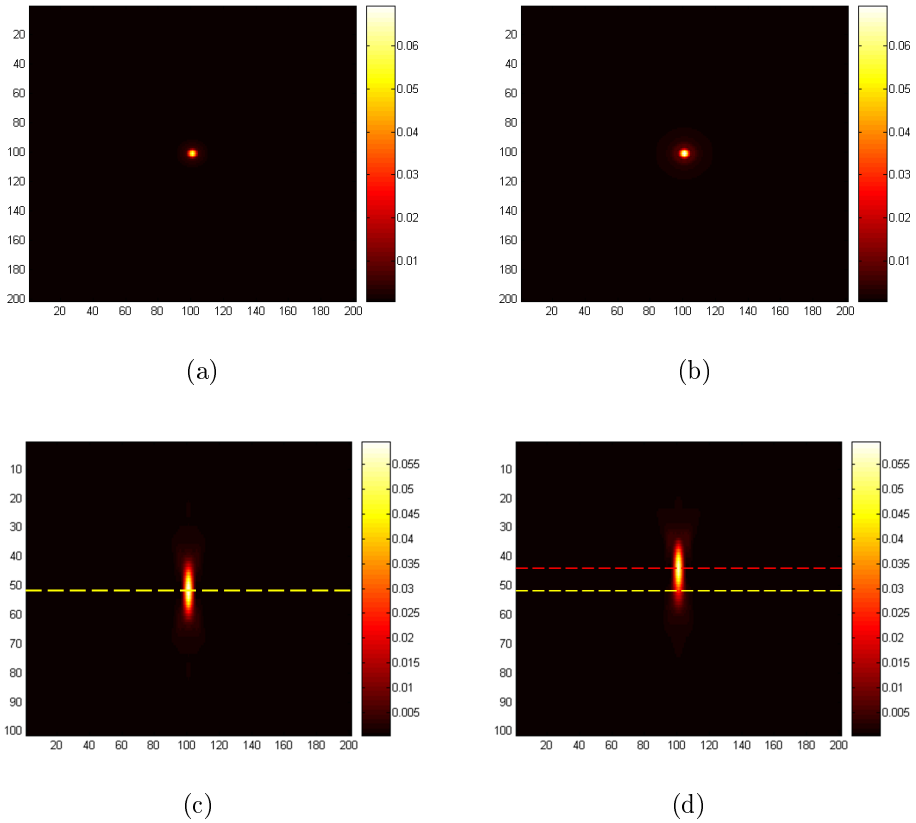

(a) (b)

(c) (d)

Figure 6: Maximum intensity projection of a numerically computed confocal laser scanning PSF (a) along the lateral plane giving the axial plane for a zero depth, (b) along the lateral plane giving the axial plane for a depth of 4800 *nm*, (c) along the optical axis giving the radial plane for a zero depth and (d) along the optical axis giving the radial plane for a depth of 4800 *nm*.

4.2.2 Object estimation

We test the proposed restoration algorithm on the simulated micro-sphere image. For the approximate observation model, we consider two PSF generated at the bead positions, using the Stokseth PSF model (see (Stokseth [1969], Pankajakshan et al. [2009])). That is to say, the first PSF was generated at a depth of 1440 nm and the second one was generated at a depth of 3360 nm. We thus split the image volume into two overlapping sub-volumes with a recovery rate about 33% of the sub-image volume. As it is described in the second section of this report, the boundary effects are controlled by weighting functions varying along the z-axis. They were chosen as the plots exposed in Fig. 2. We considered likewise this splitting in the restoration algorithm. The regularizing parameter was set to $\alpha = 10^{-4}$. The algorithm contributes to the restored image whose axial slice is depicted in Fig. 7(c). To see the contribution of the proposed restoration method, we also present in Fig. 7(d) the result of deconvolution with a space-invariant PSF using method described in (Fornasier et al. [2009]). In order to clearly see the advantage of the proposed restoration method, we show in Fig. 8 the plots of the intensity profiles along the optical axis passing through the bead center. The red curve corresponds to the intensity profile of the original object, the green curve corresponds to the observation intensity profile, the blue curve corresponds to the restored object with space non-invariance approach and the discontinuous black curve shows the intensity profile of a restored object with the space-invariance assumption.

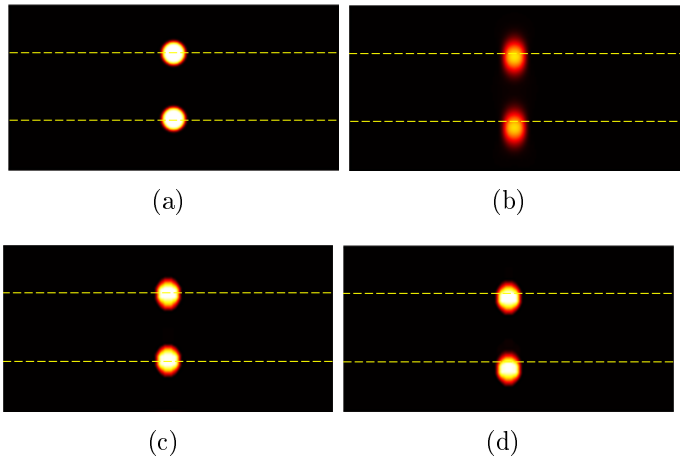

Figure 7: (a) Axial slice of the simulated 3D image of two micro-spheres, the first micro-sphere is situated at a depth of 1440 nm and the second one is situated at a depth of 3360 nm, (b) axial slice of the observation blurred with a depth-variant PSF, (c) axial slice of the restored object with the proposed restoration method considering two PSF generated at the bead positions and (d) axial slice of the restored object with space-invariant PSF generated at a zero depth.

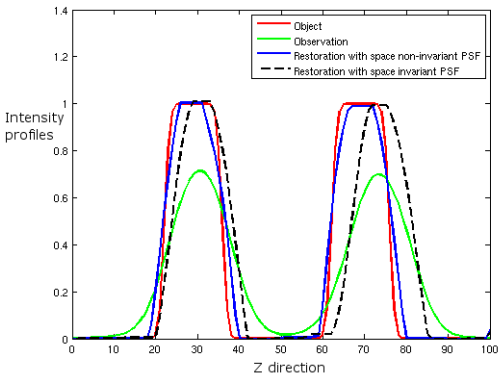

Figure 8: Intensity profiles along the optical axis passing through the center of the micro-spheres. The red plot corresponds to the original object, the green plot corresponds to the blurred object, the blue plot corresponds to the restored object with the space-variant restoration approach and the discontinuous black plot corresponds to the restored object with space-varying PSF.

5 Conclusion

In this report, we presented a restoration method for spatially-variant blurred images. We considered a block constant PSF model. In this modeling, blocking artifacts are managed thanks to an overlapping domain decomposition strategy as well as the introduction of appropriate transition functions. Furthermore, object estimation within a framework of the considered space-varying PSF was achieved by minimizing a quadratic functional including a total variation regularization. For that matter, we extended an optimization method based on an overlapping domain decomposition technique to the case of space-varying PSF. Computational time is thus reduced by performing a parallel processing on different areas of the image at the same time. The convergence of the proposed method when using a space-varying PSF model was also proved thanks to certain constraints on the considered transition functions. In fact, the proposed algorithm works for any convex combination of stationary convolution operators and thus avoids the fastidious computation in the spatial domain when filtering with space-varying filter. Indeed, in the proposed blur modeling, stationary convolutions can be rapidly computed in the Fourier domain and then combined together using space-varying weighting functions. Numerical experiments show the efficiency of the proposed restoration method and the potential interest of the space-varying PSF model. Besides, we should emphasis that the accuracy of the restored image is highly dependent on the choice of a convenient domain decomposition considered in the observation model. In fact, in each sub-domain where the blur-variation could be considered as insignificant, we consider a single approximate PSF. Automatic domain decomposition can be obtained by tolerating certain variation rate of the PSF within a given region, as it was previously proposed in (Maalouf [2010]). In that method, a correlation coefficient between a reference PSF and each of the PSF measured at different points, was computed in order to measure the PSF variation rate and then used to define PSF positions.

Several directions could extend the presented work. In fact, in our deconvolution procedure, we interested in minimizing a criterion including a data term computed as a quadratic error between the actual acquisition and the observation according to the considered model. This data term corresponds perfectly to an additive Gaussian noise context. However, if we deal with a multiplicative noisy image (e.g. Poisson noise), the energy function cannot be written in a surrogate function form (see (10)). Hence, it could be interesting to fit the proposed restoration method to the multiplicative noise case. Moreover, in the presented deconvolution method, we considered only one regularizing term which corresponds to total variation. It could be inter-

esting to incorporate other regularizing terms such as wavelet regularization mainly to avoid the staircase artifacts introduced by total variation. In that case, one should study the splitting of the regularizing criterion as it was previously done in (Fornasier et al. [2009]) for the total variation term. To conclude, blind restoration in the context of the space-varying PSF model is still an open issue.

Acknowledgment

This work has been conducted with the partial financial support of ANR Defis DIAMOND. The authors gratefully acknowledge all the partners of this ANR project for the interesting discussions and for clarifying many optical phenomena related to the confocal laser scanning microscopy.

References

J. Bardsley, S. Jefferies, J. Nagy, and R. Plemmons. A computational method for the restoration of images with an unknown spatially-varying blur. *Optics Express*, 14(5):1767–1782, 2006. ISSN 1094-4087.

H.H. Bauschke, J.M. Borwein, and A.S. Lewis. The method of cyclic projections for closed convex sets in hilbert space. In *Recent developments in optimization theory and nonlinear analysis*.

J. Bect, L. Blanc-Féraud, G. Aubert, and A. Chambolle. A l1-unified variational framework for image restoration. volume 3024, pages 1–13, Prague, Czech Republic, 2004.

A. Chambolle. An algorithm for total variation minimization and applications. *Journal of Mathematical Imaging and Vision*, 20(1):89–97, 2004. ISSN 0924-9907.

A. Chambolle and P. L. Lions. Image recovery via total variation minimization and related problems. *Numerische Mathematik*, 76(2):167–188, 1997. ISSN 0029-599X.

I. Daubechies, M. Defrise, and C. De Mol. An iterative thresholding algorithm for linear inverse problems with a sparsity constraint. *Communications on pure and applied mathematics*, 57(11):1413–1457, 2004. ISSN 1097-0312.

G. Demoment. Image reconstruction and restoration: Overview of common estimation structures and problems. *EEE Transactions on Acoustics, Speech and Signal Processing*, 37(12):2024–2036, 1989. ISSN 0096-3518.

M.A.T. Figueiredo and R.D. Nowak. An EM algorithm for wavelet-based image restoration. *IEEE Transactions on Image Processing*, 12(8):906–916, 2003. ISSN 1057-7149.

M. Fornasier and C.B. Schönlieb. Subspace correction methods for total variation and l1 minimization. *SIAM Journal on Numerical Analysis*, 47: 3397, 2009.

M. Fornasier, A. Langer, and C.B. Schönlieb. A convergent overlapping domain decomposition method for total variation minimization. *Numerische Mathematik*, pages 1–41, 2009.

N. Hajlaoui, C. Chaux, G. Perrin, F. Falzon, and A. Benazza-Benyahia. Satellite image restoration in the context of a spatially varying point spread function. *JOSA A*, 27(6):1473–1481, 2010. ISSN 1520-8532.

S. Inoué. Foundations of confocal scanned imaging in light microscopy. *Handbook of biological confocal microscopy*, pages 1–19, 2006.

E. Maalouf. Contribution to fluorescence microscopy, 3d thick samples deconvolution and depth-variant psf. In *Ph.D. thesis, UHA*, Mulhouse, France, 2010.

M. Minsky. Memoir on inventing the confocal microscope. *Scanning*, 10: 128–138, 1988.

J.G. Nagy and D.P. O'Leary. Restoring images degraded by spatially variant blur. *SIAM Journal on Scientific Computing*, 19(4):1063–1082, 1998. ISSN 1064-8275.

J.G. Nagy, R.J. Plemmons, and T.C. Torgersen. Iterative image restoration using approximate inverse preconditioning. *IEEE Transactions on Image Processing*, 5(7):1151–1162, 1996.

P. Pankajakshan, B. Zhang, L. Blanc-Féraud, Z. Kam, J.C. Olivo-Marin, and J. Zerubia. Blind deconvoltion for thin layered confocal imaging. *Applied Optics*, 48(22):4437–4448, 2009.

J.B. Pawley. Fundamental limits in confocal microscopy. *Handbook of Biological Confocal Microscopy*, pages 0–42, 2006.

W.K. Pratt. Generalized wiener filtering computation techniques. *EEE Transactions on Computers*, pages 636–641, 1972.

C. Preza and J.A. Conchello. Depth-variant maximum-likelihood restoration for three-dimensional fluorescence microscopy. *JOSA A*, 21(9):1593–1601, 2004. ISSN 1520-8532.

L.I. Rudin and S. Osher. Total variation based image restoration with free local constraints. In *IEEE International Conference on Image Processing*, volume 1, pages 31–35, Austin, TX, USA, 1994. ISBN 0818669527.

L.I. Rudin, S. Osher, and E. Fatemi. Nonlinear total variation based noise removal algorithms. *Physica D: Nonlinear Phenomena*, 60(1-4):259–268, 1992. ISSN 0167-2789.

J.W. Shaevitz and D.A. Fletcher. Enhanced three-dimensional deconvolution microscopy using a measured depth-varying point-spread function. *JOSA A*, 24(9):2622–2627, 2007.

P.A. Stokseth. Properties of a defocused optical system. *JOSA*, 59(10): 1314–1321, 1969.

H. K. Sung and H. M. Choi. Nonlinear restoration of spatially varying blurred images using self-organizing neural network. In *IEEE International Conference on Acoustics, Speech, and Signal Processing*, volume 2, pages 1097–1100, Seattle, WA , USA, 1998.

Centre de recherche INRIA Sophia Antipolis – Méditerranée
2004, route des Lucioles - BP 93 - 06902 Sophia Antipolis Cedex (France)

Centre de recherche INRIA Bordeaux – Sud Ouest : Domaine Universitaire - 351, cours de la Libération - 33405 Talence Cedex
Centre de recherche INRIA Grenoble – Rhône-Alpes : 655, avenue de l'Europe - 38334 Montbonnot Saint-Ismier
Centre de recherche INRIA Lille – Nord Europe : Parc Scientifique de la Haute Borne - 40, avenue Halley - 59650 Villeneuve d'Ascq
Centre de recherche INRIA Nancy – Grand Est : LORIA, Technopôle de Nancy-Brabois - Campus scientifique
615, rue du Jardin Botanique - BP 101 - 54602 Villers-lès-Nancy Cedex
Centre de recherche INRIA Paris – Rocquencourt : Domaine de Voluceau - Rocquencourt - BP 105 - 78153 Le Chesnay Cedex
Centre de recherche INRIA Rennes – Bretagne Atlantique : IRISA, Campus universitaire de Beaulieu - 35042 Rennes Cedex
Centre de recherche INRIA Saclay – Île-de-France : Parc Orsay Université - ZAC des Vignes : 4, rue Jacques Monod - 91893 Orsay Cedex

Éditeur
INRIA - Domaine de Voluceau - Rocquencourt, BP 105 - 78153 Le Chesnay Cedex (France)
http://www.inria.fr
ISSN 0249-6399